

A hybrid mathematical model of solid tumour invasion: the importance of cell adhesion

ALEXANDER R. A. ANDERSON[†]

*Division of Mathematics, University of Dundee,
Dundee DD1 4HN, UK*

[Received on 9 December 2003; revised on 21 July 2004; accepted on 30 November 2004]

In this paper we present a hybrid mathematical model of the invasion of healthy tissue by a solid tumour. In particular we consider early vascular growth, just after angiogenesis has occurred. We examine how the geometry of the growing tumour is affected by tumour cell heterogeneity caused by genetic mutations. As the tumour grows, mutations occur leading to a heterogeneous tumour cell population with some cells having a greater ability to migrate, proliferate or degrade the surrounding tissue. All of these cell properties are closely controlled by cell–cell and cell–matrix interactions and as such the physical geometry of the whole tumour will be dependent on these individual cell interactions. The hybrid model we develop focuses on four key variables implicated in the invasion process: tumour cells, host tissue (extracellular matrix), matrix-degradative enzymes and oxygen. The model is considered to be hybrid since the latter three variables are continuous (i.e. concentrations) and the tumour cells are discrete (i.e. individuals). With this hybrid model we examine how individual-based cell interactions (with one another and the matrix) can affect the tumour shape and discuss which of these interactions is perhaps most crucial in influencing the tumour's final structure.

1. Introduction

The development of a primary solid tumour (e.g. a carcinoma) begins with a single normal cell becoming transformed as a result of mutations in certain key genes. This transformed cell differs from a normal one in several ways, one of the most notable being its escape from the body's homeostatic mechanisms, leading to inappropriate proliferation. An individual tumour cell has the potential, over successive divisions, to develop into a cluster (or nodule) of tumour cells. Further growth and proliferation leads to the development of an avascular tumour consisting of approximately 10^6 cells. Since the tumour is dependent on diffusion as the only means of receiving nutrients and removing waste products, its growth is limited. For any further development to occur the tumour must initiate angiogenesis—the recruitment of blood vessels from a pre-existing vascular network. Once angiogenesis is complete, the perfused vascular network can supply the tumour with the nutrients it needs to grow further. There is also now the possibility of tumour cells finding their way into the circulatory system (via the vascular network) and being deposited at distant sites in the body, resulting in metastases (secondary tumours). Clearly angiogenesis, the process which results in the tumour having a vascular network, is a key process for metastatic invasion.

Central to the invasive process are the molecules that facilitate interactions between cells and between cells and the *extracellular matrix* (ECM), known as cell adhesion molecules. A common feature of cell adhesion molecules is their ability to function as a molecular bridge between an external ligand and the cytoskeleton within the cell (Burrige & Chrzanowska-Wodnicka, 1996). Over the past

[†]Email: anderson@maths.dundee.ac.uk

few years, it has become clear that receptors that mediate cell adhesion do not just affect cell migration, since occupancy of cell-surface receptors results in the initiation of signal-transduction pathways that regulate many aspects of cell function (Burrige & Chrzanowska-Wodnicka, 1996; Hynes, 1992), including transcription, proliferation, differentiation, cytoskeletal organisation and receptor activation (Clark & Brugge, 1995).

A crucial part of the invasive/metastatic process is the ability of the cancer cells to degrade the surrounding tissue or ECM (Liotta *et al.*, 1983; Stetler-Stevenson *et al.*, 1993; Lawrence & Steeg, 1996). This extracellular material is a complex mixture of macromolecules (MM), some of which, like the collagens, play a structural role and others, such as laminin, fibronectin and vitronectin, are important for cell adhesion, spreading and motility. We note that all of these MM are *bound* within the tissue, i.e. they are non-diffusible. The ECM can also sequester growth factors and itself be degraded to release fragments which can have growth-promoting activity. Thus, while ECM may have to be physically removed in order to allow a tumour to spread, its degradation may, in addition, have biological effects on tumour cells.

A number of *matrix-degradative enzymes* (MDEs) such as the *plasminogen activator* (PA) system and the large family of *matrix metalloproteinases* (MMPs) have been described (Matrisian, 1992; Mignatti & Rifkin, 1993; Thorgeirsson *et al.*, 1994) and both of these have been repeatedly implicated in tumour invasion and metastasis. In addition to opening migratory pathways, MDEs can alter cell adhesion properties regulated through several classes of cell-surface receptors. These receptors, including cadherins, CD-44, integrins and receptors for fibronectin, laminin and vitronectin, negatively regulate cell motility and growth through cell-cell and cell-matrix interactions (Stetler-Stevenson *et al.*, 1993). Therefore, proteolytic degradation of receptor and/or ECM components could release tumour cells from these constraints. Recent studies have shown that CD-44 mediates the attachment of cells to various MM (Radotra *et al.*, 1994). In fact, invasion of human glioma cells has been inhibited by antibodies against CD-44 (Koochekpour *et al.*, 1995). It is therefore important for any model that considers tumour invasion to include both cell-cell and cell-matrix interactions.

Tumour heterogeneity at the genetic level is well known. A mutation in the p53 gene, the so-called 'Guardian of the Genome', is widely considered as a precursor to much wider genetic variation (Lane, 1994). The p53 protein links three cellular functions: proliferation, death and DNA repair. In normal cells, p53 blocks proliferation and enables damaged DNA to be repaired. If DNA repair is incomplete, then apoptosis is initiated and the cell dies. Loss of p53 function (e.g. through mutation) allows for the propagation of damaged DNA to daughter cells (Barnes *et al.*, 1993; Lane, 1994). Whilst p53 mutations do not occur in all tumours it has been estimated that on average 50% of all human tumours have p53 mutations, although, it depends very much upon the tissue in which the tumour originated, e.g. in lung cancer the p53 mutation rate is 75%, whereas in breast cancer it is only 30% (Slee *et al.*, 2004). It has also been shown that in some cancers the incidence of p53 mutations increases with the stage of the tumours progression (Boyle *et al.*, 1993).

As a step towards the inclusion of true tumour heterogeneity we shall consider a tumour that has phenotypic heterogeneity, with p53 being the only specific gene considered. Its effect is simply to allow the genetic mutations to begin and of course to allow the tumour cell to survive. The tumour cell phenotype will be defined here by the level of the cell's aggressiveness, i.e. a combination of its cell-cell adhesiveness, proliferation, degradation and migration rates (further details will be discussed below).

Over the last 10 years or so, many mathematical models of tumour growth, both temporal and spatio-temporal, have appeared in the research literature (see Chaplain, 1996, for a review of many of these). Much of the experimental data that exist on the growth kinetics of avascular tumours have been

incorporated into mathematical models using various growth laws such as Gompertzian growth, logistic growth and exponential growth, to name but a few (see, e.g. Wheldon, 1986; Retsky *et al.*, 1990; Marusic *et al.*, 1994, and references therein). Modelling of the important process of tumour-induced angiogenesis and capillary network formation has also been undertaken (Chaplain, 1996; Anderson & Chaplain, 1998). Deterministic reaction–diffusion equations have been used to model the spatial spread of tumours both at an early stage in its growth (Sherratt & Nowak, 1992; Ward & King, 1999) and at the later invasive stage (Orme & Chaplain, 1996; Gatenby & Gawlinski, 1996; Perumpanani *et al.*, 1996; Anderson *et al.*, 2000). Typical solutions observed in all these models (Orme & Chaplain, 1996; Gatenby & Gawlinski, 1996; Perumpanani *et al.*, 1996; Byrne *et al.*, 1999) appear as invading travelling waves of cancer cells. An alternative framework is to adopt a continuum/solid mechanics approach or a mechano-chemical modelling approach (Chaplain & Sleeman, 1993; Tracqui, 1995) and to consider physical pressure and forces between cells and matrix. Whilst these models are able to capture the tumour structure at the tissue level, they fail to describe the tumour at the cellular level and subsequently the subcellular level. On the other hand, cellular automata models provide such a description and allow a more realistic stochastic approach at both the cellular (Kimmel & Axelrod, 1991; Smolle & Stettner, 1993; Qi *et al.*, 1993; Anderson & Pitcairn, 2003; Kansal *et al.*, 2000; Dormann & Deutsch, 2002) and subcellular levels (Düchting, 1990; Düchting *et al.*, 1996).

The model presented in this paper is of a different type: we classify this as ‘hybrid’, since a continuum deterministic model (based on a system of reaction–diffusion–chemotaxis equations) controls the chemical/ECM dynamics and a discrete cellular automata-like model (based on a biased random-walk model) controls the cell migration and interaction. Initially, we define a system of coupled non-linear partial differential equations to model tumour invasion of surrounding tissue. We then use a discretised form of the partial differential equation governing cell migration as the basis for the hybrid discrete-continuum model. This then enables specific cell properties to be modelled at the level of the individual cell, we shall consider proliferation, death, cell–cell adhesion, mutation and production/degradation at the individual cell level. The crucial point of this technique is that it allows cells to be treated as discrete individuals and the cell processes to be modelled at the level of the cell whilst allowing the chemicals/ECM to be treated as continuous. Certain cell processes, however, such as cell–cell adhesion, would be difficult, if not impossible, to model at the continuum level. Even though the simulations presented in this paper consider up to 160,000 individual cells, the results obtained are driven explicitly by local interactions between cells and between cells and the ECM and could not be recovered from a purely continuum model.

The aim of this paper is to examine the effects of tumour cell heterogeneity upon the overall spatial structure of the tumour and to discuss the importance of the roles of cell–cell and cell–matrix interactions. To ensure that the manner in which we model tumour cell mutation is not the controlling factor in the resulting tumour heterogeneity, we consider two different mutation algorithms, (i) linear mutations and (ii) random mutations. Further details will be discussed in later sections.

2. The PDE model of invasion

We will base our mathematical model on the growth of a generic solid tumour, which we will assume has just been vascularised, i.e. a blood supply has been established. We choose to focus on four key variables involved in tumour cell invasion, thereby producing a minimal model, namely tumour cell density (denoted by n), MDE concentration (denoted by m), MM concentration (denoted by f) and oxygen concentration (denoted by c). Each of the four variables (n, m, f, c) is a function of the spatial variable \mathbf{x} and time t . Initially, we define a system of coupled non-linear partial differential equations to

model tumour invasion of surrounding tissue and use these as the basis for the hybrid discrete-continuum technique.

We will assume that the ECM consists of a mixture of MM (e.g. collagen, fibronectin, laminin and vitronectin) only and not any other cells. Most of the MM of the ECM which are important for cell adhesion, spreading and motility are *fixed* or *bound* to the surrounding tissue. As already discussed in Section 1, MDEs are important at many stages of tumour growth, invasion and metastasis, and the manner in which they interact with inhibitors, growth factors and tumour cells is very complex. However, it is well known that the tumour cells produce MDEs which degrade the ECM locally. As well as making space into which tumour cells may move by simple diffusion (random motility), we assume that this also results in a gradient of these bound cell-adhesion molecules, such as fibronectin. Therefore, while the ECM may constitute a barrier to normal cell movement, it also provides a substrate to which cells may adhere and upon which they may move. Most mammalian cell types require at least some elements of the ECM to be present for growth and survival and will indeed migrate up a gradient of bound (i.e. non-diffusible) cell-adhesion molecules in culture *in vitro* (Carter, 1965; Quigley *et al.*, 1983; Lacovara *et al.*, 1984; McCarthy & Furcht, 1984; Klominek *et al.*, 1993; Lawrence & Steeg, 1996).

By definition, haptotaxis is the directed migratory response of cells to gradients of fixed or bound chemicals (i.e. non-diffusible chemicals). While it has not yet been explicitly demonstrated that haptotaxis occurs in an *in vivo* situation, given the structure of human tissue, it is not unreasonable to assume that haptotaxis is a major component of directed movement in tumour cell invasion. Indeed, there has been much recent effort to characterise such directed movement (Klominek *et al.*, 1993; Lawrence & Steeg, 1996; Debruyne *et al.*, 2002). We therefore refer to this directed movement of tumour cells in our model as haptotaxis, i.e. a response to gradients of bound MM such as fibronectin. To incorporate this response in our mathematical model, we take the haptotactic flux to be $\mathbf{J}_{\text{hapto}} = \chi n \nabla f$, where $\chi > 0$ is the (constant) haptotactic coefficient.

As mentioned above, the only other contribution to tumour cell motility in our model is assumed to be random motion. To describe the random motility of the tumour cells, we assume a flux of the form $\mathbf{J}_{\text{rand}} = -D_n \nabla n$, where D_n is the constant random motility coefficient.

We only model the tumour cell migration at this level as all other tumour cell processes, such as proliferation, adhesion and death, will be considered at the single cell level within the hybrid discrete-continuum model. The conservation equation for the tumour cell density n is therefore given by

$$\frac{\partial n}{\partial t} + \nabla \cdot (\mathbf{J}_{\text{rand}} + \mathbf{J}_{\text{hapto}}) = 0,$$

and hence the partial differential equation governing tumour cell motion (in the absence of cell proliferation) is

$$\frac{\partial n}{\partial t} = D_n \nabla^2 n - \chi \nabla \cdot (n \nabla f). \quad (1)$$

The ECM is known to contain many MM, including fibronectin, laminin and collagen, which can be degraded by MDEs (Stetler-Stevenson *et al.*, 1996; Chambers & Matrisian, 1997). We assume that the MDEs degrade ECM upon contact and hence the degradation process is modelled by the following simple equation:

$$\frac{\partial f}{\partial t} = -\delta m f, \quad (2)$$

where δ is a positive constant.

Active MDEs are produced (or activated) by the tumour cells, diffuse throughout the tissue and undergo some form of decay (either passive or active). The equation governing the evolution of MDE concentration is therefore given by:

$$\frac{\partial m}{\partial t} = D_m \nabla^2 m + g(n, m) - h(n, m, f), \tag{3}$$

where D_m is a positive constant, the MDE diffusion coefficient, g is a function modelling the production of active MDEs by the tumour cells and h is a function modelling the MDE decay. For simplicity we assume that there is a linear relationship between the density of tumour cells and the level of active MDEs in the surrounding tissues (regardless of the amount of enzyme precursors secreted and the presence of endogenous inhibitors) and so these functions are taken to be $g = \mu n$ (MDE production by the tumour cells) and $h = \lambda m$ (natural decay), respectively.

As already discussed in Section 1, it is well known that solid tumours need oxygen to grow and invade. Oxygen is assumed to diffuse into the MM, decay naturally and be consumed by the tumour. For simplicity oxygen production is proportional to the MM density. This is a crude way of modelling an angiogenic oxygen supply, see Anderson & Chaplain (1998) for a more appropriate way of modelling the angiogenic network. The oxygen equation therefore has the form,

$$\frac{\partial c}{\partial t} = D_c \nabla^2 c + \beta f - \gamma n - \alpha c, \tag{4}$$

where $D_c, \beta, \gamma, \alpha$ are positive constants representing the oxygen diffusion coefficient, production, uptake and natural decay rates, respectively. Necrosis (cell death induced by lack of oxygen) will occur in our model if the oxygen concentration falls below a critical level; however, since this is considered as an individual-based process it will be discussed in more detail in the hybrid discrete-continuum model section below.

The complete system of equations describing the interactions of the tumour cells, MM, MDEs and oxygen as detailed in the previous paragraphs is

$$\begin{aligned} \frac{\partial n}{\partial t} &= \overbrace{D_n \nabla^2 n}^{\text{random motility}} - \overbrace{\chi \nabla \cdot (n \nabla f)}^{\text{haptotaxis}}, \\ \frac{\partial f}{\partial t} &= - \overbrace{\delta m f}^{\text{degradation}}, \\ \frac{\partial m}{\partial t} &= \overbrace{D_m \nabla^2 m}^{\text{diffusion}} + \overbrace{\mu n}^{\text{production}} - \overbrace{\lambda m}^{\text{decay}}, \\ \frac{\partial c}{\partial t} &= \overbrace{D_c \nabla^2 c}^{\text{diffusion}} + \overbrace{\beta f}^{\text{production}} - \overbrace{\gamma n}^{\text{uptake}} - \overbrace{\alpha c}^{\text{decay}}, \end{aligned} \tag{5}$$

where D_n, D_m and D_c are the tumour cell, MDE and oxygen diffusion coefficients, respectively, χ is the haptotaxis coefficient and $\delta, \mu, \lambda, \beta, \gamma$ and α are positive constants. We should also note that cell–matrix adhesion is modelled here by the use of haptotaxis in the cell equation, i.e. directed movement up gradients of MM. Therefore, χ maybe considered as relating to the strength of the cell–matrix adhesion.

This system is considered to hold on some square spatial domain Ω (a region of tissue) with appropriate initial conditions for each variable. We assume that the MM, oxygen, tumour cells and consequently

the MDEs remain within the domain of tissue under consideration and therefore no-flux boundary conditions are imposed on $\partial\Omega$, the boundary of Ω .

2.1 Non-dimensionalisation and parameterisation

In order to use realistic parameter values, we first of all non-dimensionalise the equations in the standard way. We rescale distance with an appropriate length scale L (e.g. the maximum invasion distance of the cancer cells at this early stage of invasion, approximately 1 cm), time with τ (e.g. the average time taken for mitosis to occur, approximately 8–24 h, Calabresi & Schein, 1993), tumour cell density with n_0 , ECM density with f_0 , MDE concentration with m_0 and oxygen concentration with c_0 (where n_0 , f_0 , m_0 and c_0 are appropriate reference variables). Therefore, setting

$$\tilde{n} = \frac{n}{n_0}, \quad \tilde{f} = \frac{f}{f_0}, \quad \tilde{m} = \frac{m}{m_0}, \quad \tilde{c} = \frac{c}{c_0}, \quad \tilde{\mathbf{x}} = \frac{\mathbf{x}}{L}, \quad \tilde{t} = \frac{t}{\tau},$$

in (5) and dropping the tildes for notational convenience, we obtain the scaled system of equations:

$$\begin{aligned} \frac{\partial n}{\partial t} &= \overbrace{d_n \nabla^2 n}^{\text{random motility}} - \overbrace{\rho \nabla \cdot (n \nabla f)}^{\text{haptotaxis}}, \\ \frac{\partial f}{\partial t} &= - \overbrace{\eta m f}^{\text{degradation}}, \\ \frac{\partial m}{\partial t} &= \overbrace{d_m \nabla^2 m}^{\text{diffusion}} + \overbrace{\kappa n}^{\text{production}} - \overbrace{\sigma m}^{\text{decay}}, \\ \frac{\partial c}{\partial t} &= \overbrace{d_c \nabla^2 c}^{\text{diffusion}} + \overbrace{v f}^{\text{production}} - \overbrace{\omega n}^{\text{uptake}} - \overbrace{\phi c}^{\text{decay}}, \end{aligned} \tag{6}$$

where $d_n = \tau D_n / L^2$, $\rho = \tau \chi f_0 / L^2$, $\eta = \tau m_0 \delta$, $d_m = \tau D_m / L^2$, $\kappa = \tau \mu n_0 / m_0$, $\sigma = \tau \lambda$, $d_c = \tau D_c / L^2$, $v = \tau f_0 \beta / c_0$, $\omega = \tau n_0 \gamma / c_0$, $\phi = \tau \alpha$.

The cell cycle time can be highly variable (particularly the G1 phase) and really depends on the specific tumour under consideration. As a rough guide we take $\tau = 16$ h, halfway between 8–24 h (Calabresi & Schein, 1993). The cell motility parameter $D_n \sim 10^{-9}$ cm² s⁻¹ was estimated from available experimental evidence (Bray, 1992). Tumour cell diameters again will vary depending on the type of tumour being considered but are in the range 10–100 μ m (Melicow, 1982) with an approximate volume of 10^{-9} to 3×10^{-8} cm³ (Folkman & Hochberg, 1973; Casciari *et al.*, 1992). We will assume that a tumour cell has the volume 1.5×10^{-8} cm³ and therefore take $n_0 = 6.7 \times 10^7$ cells cm⁻³. The haptotactic parameter $\chi \sim 2600$ cm² s⁻¹ M⁻¹ was estimated to be in line with that calculated in Anderson *et al.* (2000) and the parameter $f_0 \sim 10^{-8}$ – 10^{-11} M was taken from the experiments of Terranova *et al.* (1985). We took D_m to be 10^{-9} cm² s⁻¹, which is perhaps small for a diffusing chemical, but recent experimental evidence implies that it is in fact a combination of the MDE and MM, which results in degradation of the MM and that this bound chemical diffuses very little (Hotary *et al.*, 2000). An *in vivo* estimate for the MDE concentration m_0 is somewhat difficult to obtain since there is currently no published value (that we are aware of) and we also know that certain inhibitors (e.g. tissue inhibiting metalloproteases) are produced within the ECM which will affect the MDE concentration. Plasma levels of specific MDEs have been measured (e.g. MMP-2, Zervoudaki *et al.*, 2004) and are

approximately 130 ng ml^{-1} with further increases observed in patients with cancer (Johansson *et al.*, 2000). How this relates to the MDE concentration within the ECM is not clear, we have therefore left this parameter undefined. Estimates for the kinetic parameters μ , λ and δ were not available since these are very difficult to obtain experimentally, we therefore use the values of Anderson *et al.* (2000). Oxygen is known to diffuse through water at a rate of $D_c = 10^{-5} \text{ cm}^2 \text{ s}^{-1}$ and cells consume oxygen at a rate of $6.25 \times 10^{-17} \text{ M cells}^{-1} \text{ s}^{-1}$ (Casciari *et al.*, 1992). The background oxygen concentration within the tissue was somewhat difficult to estimate as this depends on how well the tissue is vascularised. If we take the concentration of oxygen in the blood supplying the tumour/tissue to be 0.15 ml O_2 per ml of blood and since we know that 1 M of oxygen occupies 22400 ml then there is $0.15/22400 \text{ M O}_2 \text{ ml}^{-1} = 6.7 \times 10^{-6} \text{ M O}_2 \text{ ml}^{-1}$, and since $1 \text{ ml} = 1 \text{ cm}^3$ then we calculate $c_0 = 6.7 \times 10^{-6} \text{ M O}_2 \text{ cm}^{-3}$ (Sherwood, 2001). Clearly, this would be an overestimate, since not all of the domain will be fully vascularised but this at least gives us a reference value.

3. The hybrid discrete-continuum model

The hybrid discrete-continuum technique (see Anderson *et al.*, 1997 to Anderson & Pitcairn, 2003) will be used to follow the path of an individual tumour cell and first of all involves discretising (using standard finite-difference methods) the system of partial differential equations (6). We then use the resulting coefficients of the five-point finite-difference stencil to generate the probabilities of movement of an individual cell in response to its local milieu (see Appendix of Anderson *et al.*, 2000, for the full discrete system).

As an illustration of the technique we only consider the tumour cell equation,

$$n_{i,j}^{q+1} = n_{i,j}^q P_0 + n_{i+1,j}^q P_1 + n_{i-1,j}^q P_2 + n_{i,j+1}^q P_3 + n_{i,j-1}^q P_4. \quad (7)$$

The coefficient P_0 , which is proportional to the probability of no movement, has the form

$$P_0 = 1 - \frac{4kD_n}{h^2} - \frac{k\rho}{h^2} \left(f_{i+1,j}^q + f_{i-1,j}^q - 4f_{i,j}^q + f_{i,j+1}^q + f_{i,j-1}^q \right), \quad (8)$$

and the coefficients P_1 , P_2 , P_3 and P_4 , which are proportional to the probabilities of moving left, right, down and up, respectively, have the forms

$$\begin{aligned} P_1 &= \frac{kD}{h^2} - \frac{k\rho}{4h^2} [f_{i+1,j}^q - f_{i-1,j}^q], \\ P_2 &= \frac{kD}{h^2} + \frac{k\rho}{4h^2} [f_{i+1,j}^q - f_{i-1,j}^q], \\ P_3 &= \frac{kD}{h^2} - \frac{k\rho}{4h^2} [f_{i,j+1}^q - f_{i,j-1}^q], \\ P_4 &= \frac{kD}{h^2} + \frac{k\rho}{4h^2} [f_{i,j+1}^q - f_{i,j-1}^q], \end{aligned} \quad (9)$$

where the subscripts specify the location on the grid and the superscripts the time steps, i.e. $x = ih$, $y = jh$ and $t = qk$, where i , j , k , q and h are positive parameters.

The central assumption in the hybrid discrete-continuum technique is that the five coefficients P_0 to P_4 are proportional to the probabilities of the tumour cell being stationary (P_0) or moving left (P_1), right (P_2), down (P_3) or up (P_4). From the above probabilities we see that if there were no MM, the values

of P_1 to P_4 would be equal, with P_0 smaller (or larger, depending on the precise values chosen for the space and time steps), i.e. there is no bias in any one direction and the tumour cell is less (more) likely to be stationary—approximating an unbiased random walk. However, if there are gradients in the MM, haptotaxis contributes to the migration process and the coefficients P_0 to P_4 will become biased towards the direction of increased MM concentration. The motion of an individual cell is therefore governed by its interactions with the matrix MM in its local environment. Of course, the motion will also be modified by interactions with other tumour cells.

Note that using the coefficients of the discrete cell equation as probabilities of movement is only one of many ways that movement probabilities could be defined, e.g. one could start from a reinforced random-walk model and define transition probabilities that have a random component and ‘taxis’ component which would depend on variations in ECM density. In fact, Othmer & Stevens (1997) derive a reinforced random-walk model with transition probabilities that have both of these components, classed as gradient models in their paper. They then derive a partial differential equation in the continuous limit that consists of a diffusion term and a chemotaxis term. It is possible to show this for our model by defining transition probabilities of the form P_1 to P_4 . The original equation governing the rate of change of tumour cell density (6) can then be recovered. For more details on how this can be done and on the hybrid discrete-continuum technique and its application see Anderson (2003) and Anderson & Pitcairn (2003).

Also, note that we could instead consider a nine-point finite-difference stencil to generate the probabilities of movement, whilst this would give a cell an extra four possible movements along the diagonals, it would also greatly increase the computation time. There is no obvious advantage to having nine movement probabilities as opposed to four in our simulations, with regards to migration, as the unbiased movement term (e.g. $\frac{kD}{h^2}$) insures that any grid effects (e.g. orthogonal bias) are minimal.

3.1 *Individual-based processes*

We shall now discuss in detail the processes each tumour cell will experience as it migrates through the MM field, driven by the movement probabilities defined in the previous section.

3.1.1 *Life cycle*

Figure 1 shows a flowchart of a tumour cell’s ‘life cycle’ within the hybrid discrete-continuum simulation. At each time step, a tumour cell will initially check if it can move with regards to cell–cell adhesion restrictions (see the next paragraph for criteria), if it can, then the movement probabilities (above) are calculated and the cell is moved. A check is then made if the cell should die (see Section 3.1.3 for criteria) or not. If it does not die, its age is increased and a check to see if it has reached proliferation age is performed. If it has not reached this age, then it starts the whole loop again. If proliferation age has been reached, then a check is made to see if the criteria for proliferation are satisfied (see Section 3.1.4 for details). If proliferation criteria are not met, then the cell becomes quiescent. If they are satisfied, then we check to see if this mitosis results in a p53 mutation. If a p53 mutation does not result, then death occurs, but if it does, then further mutations are possible (see Section 3.1.5 for details). This whole process is repeated at each time step of the simulation.

3.1.2 *Cell–cell adhesion*

To model cell–cell adhesion explicitly, we assume each cell has its own internal adhesion value (A_i , see Table 1), i.e. the number of neighbours that it will preferentially adhere to. We therefore examine the number of external neighbours each cell has (A_e) and if $A_e \geq A_i$, then the cell is allowed to migrate,

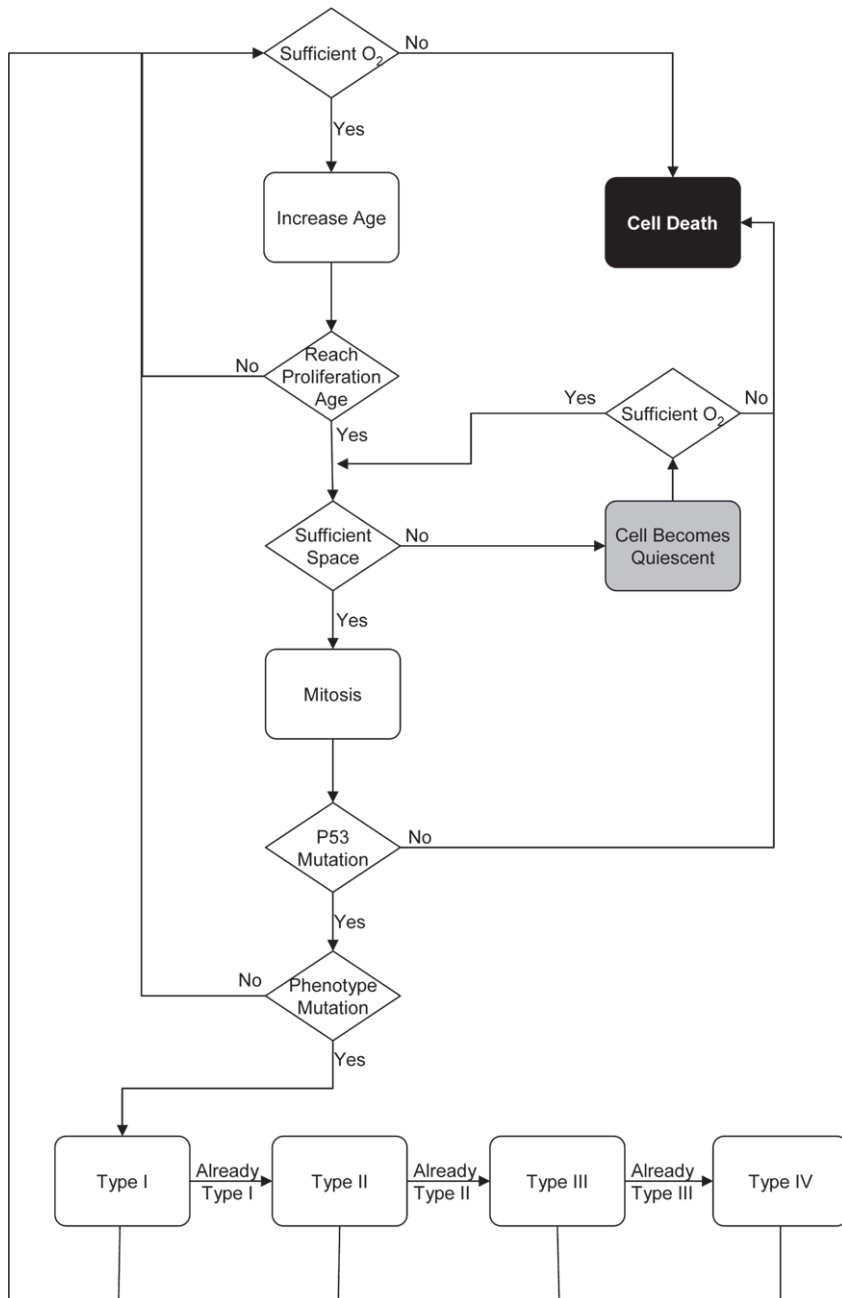


FIG. 1. Flowchart of a tumour cell life cycle within the hybrid discrete-continuum simulation. Note, a full colour version of this figure is available in the online publication.

TABLE 1 *Parameter values for each of the four different phenotypes. Colours are used to identify the different phenotypes in the simulation results below*

Phenotype	Proliferation age M	O ₂ uptake	MDE production	A_i	Haptotaxis
I (orange)	16 h	ω	κ	3	ρ
II (green)	14 h	$4/3\omega$	$4/3\kappa$	2	$4/3\rho$
III (cyan)	12 h	2ω	2κ	1	2ρ
IV (blue)	8 h	4ω	4κ	0	4ρ

otherwise it remains stationary. Whilst this is a somewhat crude way of modelling cell adhesion, it does capture some features of cell–cell adhesion, e.g. certain cells are more likely to bind to others and in so doing restrict their own ability to migrate.

3.1.3 *Death*

For the tumour cell to survive, it requires sufficient oxygen, since some tumour cells have been found to survive in very poorly oxygenated environments, we make the assumption that the concentration has to drop to 0.05 non-dimensional units (where 1 would be the initial concentration) for cell death to occur. This assumption is also applied to quiescent tumour cells. The space that dead cells occupy becomes available to new cells as soon as they die. Cell death can also occur due to apoptosis, if the cell does not undergo a p53 mutation after the first proliferation and in undergoing mutation, we assume that each cell has a probability $P_{p53} = 0.1$ of a p53 mutation. Whilst this maybe very much an overestimate of the true mutation probability, which is probably much smaller, once a p53 mutation occurs in a cell, all subsequent daughter cells will have the same mutation. Therefore, by considering smaller values of P_{p53} , we would be simply slowing down the initiation of the phenotype mutation process which once established would produce very similar simulation end results to a simulation with $P_{p53} = 0.1$. As with all the mutations considered here, they can only occur as a result of proliferation.

3.1.4 *Proliferation*

In our model we assume that each individual cell has the capacity for proliferation and will produce two daughter cells, provided: (i) the parent cell has reached maturity (M h, see Table 1) and (ii) there is sufficient space surrounding the parent cell for the two new daughter cells to occupy. In order to satisfy condition (ii), we assumed that one daughter cell replaces the parent cell and the other daughter cell will move to any one of the parent cell's four orthogonal neighbours that is empty. If more than one of the neighbouring grid points is empty, then the new cell position is chosen randomly from these points. If no empty neighbours exist, then the cell becomes quiescent and proliferation is delayed until space becomes available. We therefore do not consider the possibility that cells may push neighbouring cells to create free space in which to proliferate. Quiescent tumour cells are assumed to consume half the oxygen of tumour cells. This is based on the observation that in tumour spheroids quiescent cells certainly do consume less oxygen than proliferating cells, although since many other factors are involved, it is not clear as to precisely how much less and could in fact be up to five times less (Freyer *et al.*, 1984).

3.1.5 *Linear mutation*

Initially, all cells are assumed to have wild-type p53, i.e. non-mutated. After a p53 mutation occurs, the genome becomes unstable and is then open to many more mutations. So after the p53 mutation has occurred, the cell now has predefined phenotypic traits that describe its behaviour. For simplicity we

consider four phenotypes, each progressively more aggressive (in terms of invasiveness) than before. Table 1 shows the different values each phenotype takes and clearly type IV is the most aggressive, having the shortest proliferation age, consuming the most O_2 , producing the most MDE, having the largest haptotaxis coefficient and requiring no neighbours for migration. We have chosen to correlate tumour cell aggressiveness with proliferation age, O_2 uptake, MDE production, cell adhesion coefficient and haptotaxis coefficient. We assume that O_2 uptake, MDE production and haptotaxis coefficients all increase and the proliferation age and adhesion coefficients decrease as the tumour cell phenotype becomes increasingly aggressive. This assumption is based on mixture of fact and logic, as more aggressive cells are more likely to be less adhesive to one another, be better migrators and have a shorter proliferation age. It seems logical to assume that they will also be better at degrading the ECM and therefore produce more MDE and given all this increased activity they will consume more oxygen (cf. random mutation model, Section 4). The phenotypes defined in Table 1 are just one possible set of phenotypes, other sets could have been chosen and produced similar results (e.g. the random mutation model, Section 4), the important feature is that they have different levels of aggressiveness. Following the first p53 mutation, a cell is assigned the values of phenotype I (as defined in Table 1) and for each subsequent proliferation, there is a small probability (P_{mutat}) of further mutations occurring which will lead to phenotype II and so on in a linear fashion. All mutations are assumed to be irreversible.

3.1.6 Production/degradation/diffusion

Since we are modelling individual tumour cells, we must consider MDE production at the level of a single cell. In the continuum model (6), we have MDE production as being proportional to the tumour cell density. Now MDE is only produced at a grid point if a tumour cell is occupying that grid point. Since we have no precise parameter estimates for this production rate, we take $n = 1$ in the discrete form of the MDE equation when a tumour cell is occupying the current location and take $n = 0$ otherwise. Similarly for O_2 uptake, we take $n = 1$ (since ω is scaled as per cell) in the discrete form of the oxygen equation when a cell is consuming oxygen at the current location and $n = 0$ otherwise. Since the tumour cells occupy physical space within the ECM, we should consider how this might impact upon oxygen diffusion. It seems logical that oxygen diffusion will be reduced as the space occupied by the tumour increases, this is consistent with tumour spheroid results, i.e. as the spheroid diameter increases, the necrotic region also increases. To model this at the individual level, we assume that oxygen diffusion decreases at the grid point a tumour cell occupies, i.e. the oxygen diffusion rate at that grid point will be $d_{\text{cell}} < d_c$.

3.2 Simulation process for the hybrid discrete-continuum model

Each time step of the simulation process involves solving the discrete form of the system (6) numerically to generate the five coefficients P_0 to P_4 , (8) and (9). We then normalise these coefficients to obtain five corresponding final probabilities of motion, where normalisation simply means division by the total of the five coefficients. Probability ranges are then computed by summing the coefficients to produce five ranges, $R_0 = 0$ to P_0 and $R_i = \sum_{j=0}^{i-1} P_j$ to $\sum_{j=0}^i P_j$, where $i = 1$ to 4. We then generate a random number between 0 and 1, and depending on the range which this number falls in, the current individual tumour cell under consideration will remain stationary (R_0) or move left (R_1), right (R_2), down (R_3) or up (R_4). The larger a particular range, the greater the probability that the corresponding coefficient will be selected. Each tumour cell is therefore restricted to move to one of its four orthogonal neighbouring grid points or remain stationary at each time step.

All cells are given a unique identification number which is assigned as each new cell is produced (or is assigned initially for the first 50 cells). Each time step of the simulation involves firstly updating

all of the cells positions (via the identification number, i.e. the larger the identification number, the later the update) then secondly updating the individual-based processes for all the cells, e.g. proliferation, death and mutation. Therefore, cells are not updated simultaneously or in a left-to-right, top-to-bottom manner but as per the identification number. For the migration part of the update, the identification method gives preference to cells which have smaller identification values (since they get to move before the others do) but since the cells are distributed all over the tumour this should not introduce any visible bias. Once the cells have moved, the individual-based processes are updated and this is done again per cell identification number but this time the cells update as soon as a process occurs, e.g. proliferation, this should avoid any conflicts for space.

3.3 Linear mutation hybrid discrete-continuum model simulation results

The following simulations were carried out on a 400×400 grid, which is a discretisation of the unit square, $[0, 1] \times [0, 1]$, with a space step of $h = 0.0025$ and a time step of $k = 0.0005$. Note that with this choice of space step, each square of grid is approximately the same area as a tumour cell, i.e. $6.25 \times 10^{-6} \text{ cm}^2$ (or $1.56 \times 10^{-8} \text{ cm}^2$ as a volume, with cells of side 0.0025 cm). No-flux boundary conditions were imposed on the square grid, restricting the tumour cells, MDE, MM and oxygen to within the grid. Initially, 50 tumour cells are centred around $(0.5, 0.5)$ with an assigned phenotype I, a random age between 0–16 h, the MDE concentration is zero throughout the domain ($m(x, y) = 0$) and the oxygen concentration is taken to be one ($c(x, y) = 1$). We consider the effects, upon tumour invasion, of three different MM initial distributions: (i) homogeneous ($f(x, y) = 1$), (ii) heterogeneous ($0 \leq f(x, y) \leq 1$), with $f(x, y)$ being generated from a combination of sin and cos functions of the x and y directions and (iii) random ($0 \leq f(x, y) \leq 1$). For clarity we shall label the resulting tumour cell distributions as (i) homogeneous tumour, (ii) heterogeneous tumour and (iii) random tumour. The non-dimensional parameter values used in all the following simulations are $d_n = 0.0005$, $d_m = 0.0005$, $d_c = 0.5$, $d_{\text{cell}} = 0.25$, $\rho = 0.01$, $\eta = 50$, $\kappa = 1$, $\sigma = 0$, $\nu = 0.5$, $\omega = 0.57$ and $\phi = 0.025$. We also take the phenotype mutation probability to be $P_{\text{mutat}} = 0.1$. Other values were considered and produced similar results but for shorter or longer times depending on whether the probability was larger or smaller.

Figure 2 shows the simulation results for each of the four variables for the the homogeneous initial MM distribution at $t = 200$ time units. The tumour cell distribution shows a mainly dead central region with a thin dispersed proliferating boundary. As might be expected, it is the most aggressive cells of phenotype IV which have survived and continue to proliferate on the boundary, although a small cluster of cells has survived in the centre of the tumour. This is partly due to the fact that quiescent cells consume less oxygen and therefore allow for the diffusion of a little oxygen back into the centre of the tumour. Given more time, these cells will also die due to lack of oxygen. However, this does imply that even necrotic regions may still offer some potential for tumour cell survival (in the short term). Since the cells were invading through an initially homogeneous distribution of MM, it is perhaps not too surprising that this has produced a symmetric tumour (this symmetry is also seen in all three of the other variables). The homogeneous tumour has also produced a large number of individual cells, due to the combined effects of a faster invasion rate and subsequently access to empty space for proliferation leading to further invasion. The faster invasion is mainly driven by the cell–matrix interactions via haptotaxis, giving directed motion towards higher concentrations of MM. Since the type IV cells are on the boundary, they exploit this gradient the most by having the largest haptotaxis coefficient and no cell–cell adhesion dependence.

Figure 3 shows the simulation results for an initially heterogeneous MM distribution. The tumour cell distribution is now radically different geometrically, showing a more fingered morphology, although

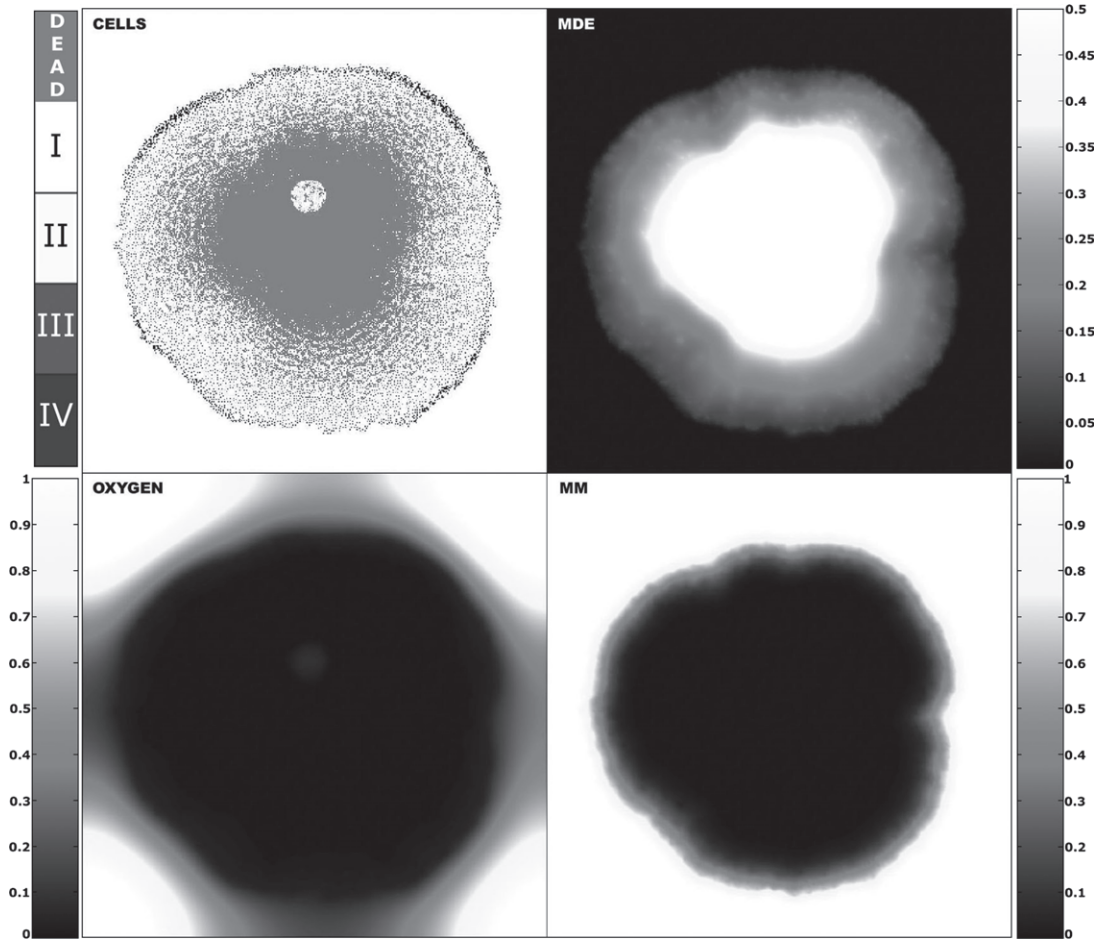


FIG. 2. Homogeneous tumour simulation results: spatial distribution of tumour cells, MDE, MM and oxygen (clockwise) at time $t = 200$ units (i.e. 200 generations, approximately 133 days). Colouration of the tumour cells represents phenotype, see colour bar for details. For the MDE, MM and oxygen concentration, the grey colour map is used, i.e. white = high concentration, black = low concentration and grey is in between. Note, a full colour version of this figure is available in the online publication.

it still consists of just two cell types, dead cells and type IV cells. Again the most aggressive cells dominate the population and lead the way for invasion at the boundary of the tumour. Since these cells have no cell–cell adhesion dependence, their migration is mainly driven by haptotaxis via the local MM gradients and it is these local gradients that ultimately define the tumour geometry. Since the initial MM distribution is somewhat artificially smooth in Figs 2 and 3, we now consider a completely random initial MM distribution in Fig. 4.

Figure 4 shows that the tumour cell distribution again displays the fingered morphology, in a slightly more symmetric manner than the heterogeneous tumour. We also see that the tumour consists of dead cells and type IV cells, again leading the invading tumour boundary.

To give a better idea of the manner in which the tumour invasion evolves in Fig. 4, we generated a series of 15 time snapshots, one every 15 time units (10 days), of the growing tumour. Figure 5 shows a

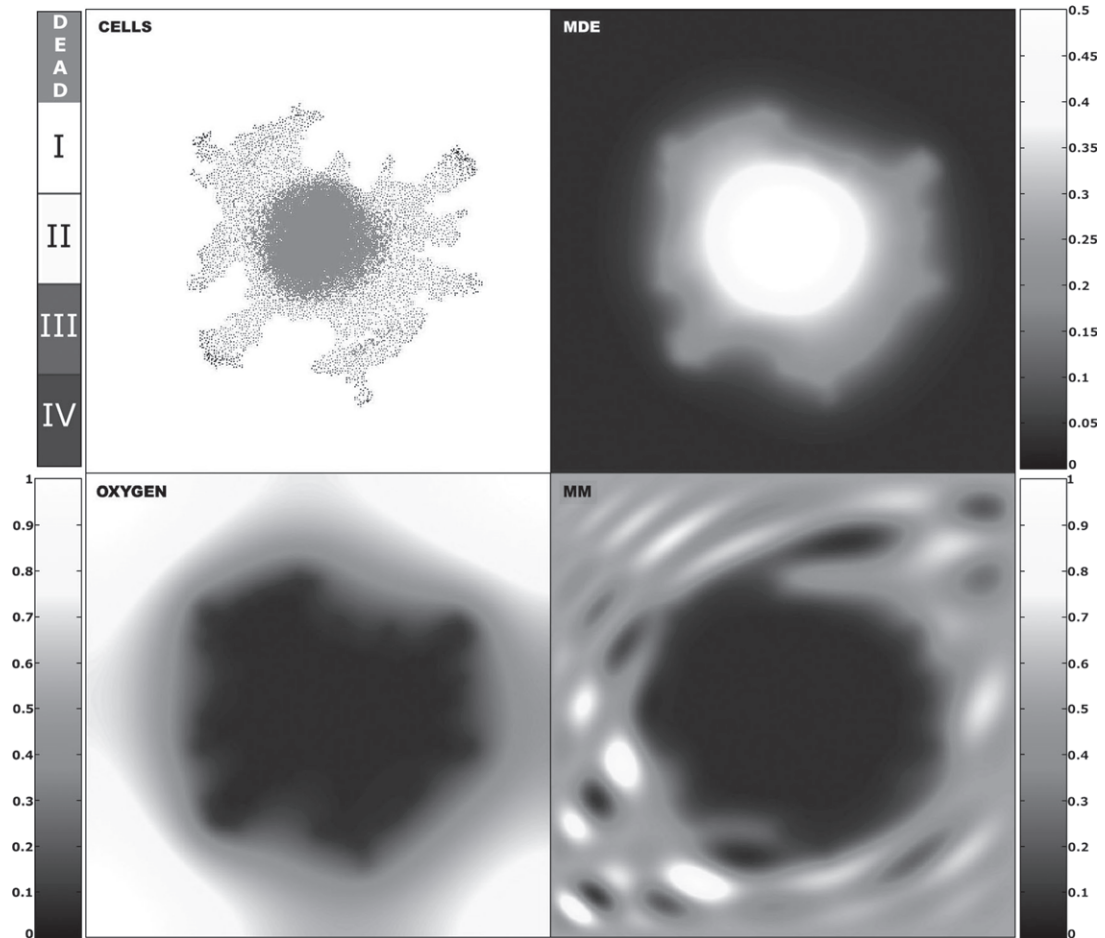


FIG. 3. Heterogeneous tumour simulation results: spatial distribution of tumour cells, MDE, MM and oxygen (clockwise) at time $t = 200$ units. Colouration as in Fig. 2.

detailed evolution of tumour invasion and we can see that the tumour, more or less, evolves as a growing disk from 4 to 75 days and is made up of a mixture of all four phenotypes as well as dead cells. However, from 85 days onwards, we begin to see the emergence of fingering and the dominance of the most aggressive type IV cells on the boundary with a dead central region. Clearly, these results emphasise the fact that it is the type IV cells that really drive the fingering and these are the cells that have no cell–cell adhesion.

Given that all three simulations above (Figs 2–5) use the same parameters, with the exception of the MM initial distributions, these results illustrate the importance of tumour cell–matrix interactions in aiding or hindering the migration of individual cells that define the tumour geometry. The fact that the resulting tumour cell populations consist of only one living cell type IV might not be surprising due to the linear nature of the mutations. However, it seems logical to assume that it will be the most aggressive tumour cells that dominate the tumour population.

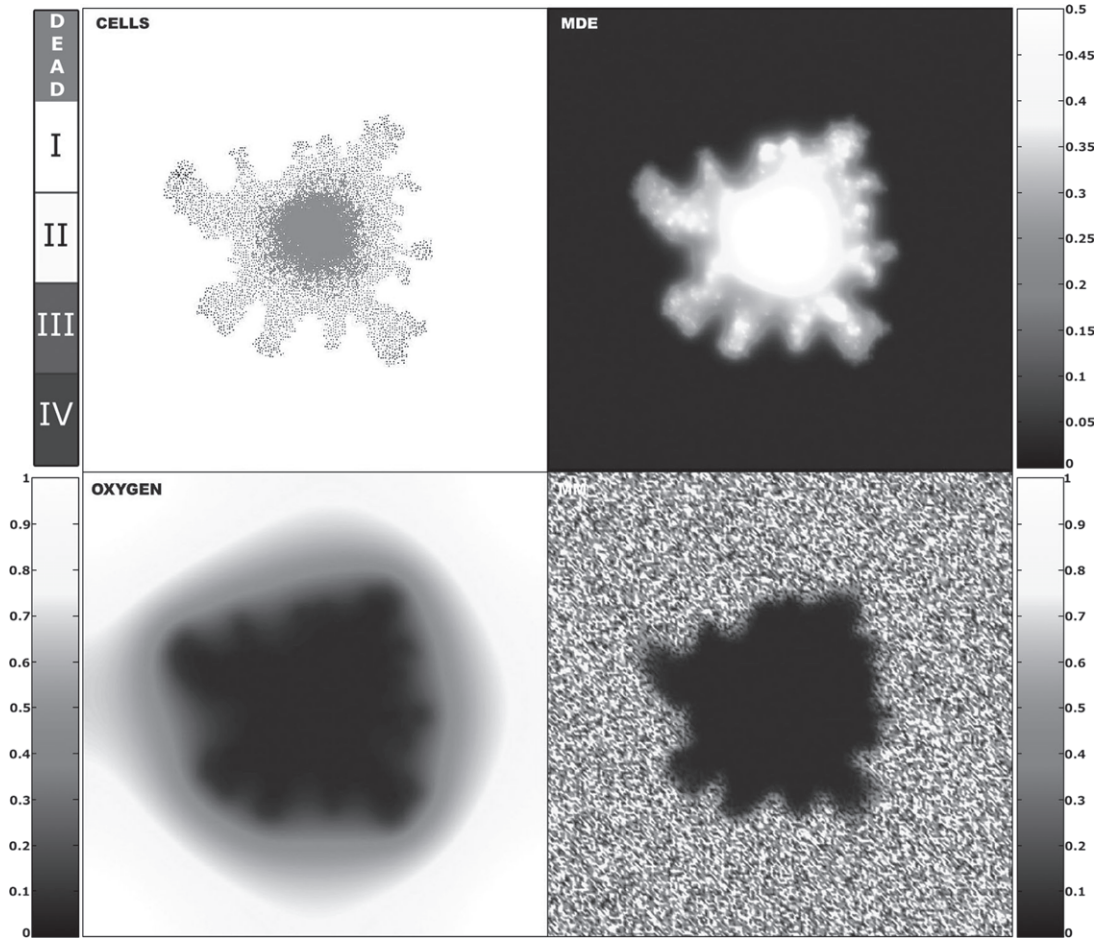


FIG. 4. Random tumour simulation results: spatial distribution of tumour cells, MDE, MM and oxygen (clockwise) at time $t = 200$ units. Colouration as in Fig. 2. Note, a full colour version of this figure is available in the online publication.

4. Random mutation hybrid discrete-continuum model

The impact of the way in which tumour cell mutation is modelled can be seen from the previous section, where the linear mutations always lead each cell to either the most aggressive phenotype (IV) or death. To gauge the effect of such a linear mutation sequence, we now consider a completely random mutation sequence and compare how these impact on the resulting tumour cell populations and overall tumour geometry.

Given that the hybrid discrete-continuum model is identical to the one above with the exception of the manner in which mutations occur, we shall only discuss how we now model random mutations.

Random mutation: Initially all cells are assumed to have wild-type p53, i.e. non-mutated. After a p53 mutation occurs, the genome becomes unstable and is then open to many more mutations (as before). So after the p53 mutation has occurred, the cell now has predefined phenotypic traits that specify its

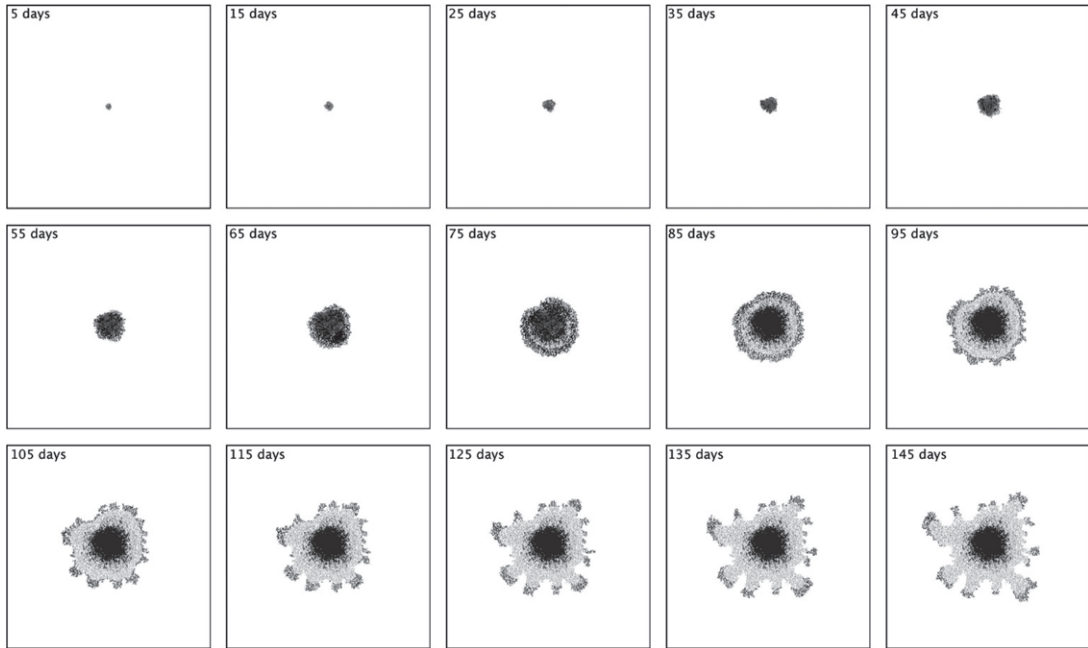


FIG. 5. Random tumour simulation results: 15 time snapshots of the spatial distribution of tumour cells at times $t = 5$ –145 days. Colouration as in Fig. 2. Note, a full colour version of this figure is available in the online publication.

behaviour. Here we shall consider 100 randomly defined phenotypes (although we could choose more or less), and each phenotype has an equal probability of being selected. We define each phenotype to be a set of parameter values that describe the behaviour of the cell expressing it. Therefore, a particular phenotype will have a randomly selected proliferation age ($\text{Phen}_{\text{age}} = 8$ –16 h), O_2 consumption ($\text{Phen}_{\text{O}_2} = \omega$ – 4ω), MDE production ($\text{Phen}_{\text{mde}} = \kappa$ – 4κ), haptotaxis coefficient ($\text{Phen}_{\text{taxis}} = \rho$ – 4ρ) and adhesion value ($\text{Phen}_{\text{A}} = 0$ –3). In most cases the range of values each parameter can take to define the phenotype were chosen to represent biologically realistic limits. Following the first p53 mutation a cell is assigned the values of one of the 100 randomly selected phenotypes and for each subsequent proliferation there is a small probability (P_{mutat}) of further mutations occurring which will lead to another randomly selected phenotype and so on.

4.1 Random mutation hybrid discrete-continuum simulation results

The following simulations were carried out on the same grid with the same parameter values, initial and boundary conditions as in Section 3.3. The only difference is that when a phenotype mutation occurs it leads to one of the randomly selected phenotypes; we again take this probability to be $P_{\text{mutat}} = 0.1$. We consider the effects, upon tumour invasion, of two different MM initial distributions: (i) homogeneous ($f(x, y) = 1$) and (ii) random ($0 \leq f(x, y) \leq 1$). For clarity we shall label the resulting tumour cell distributions as (i) homogeneous tumour and (ii) random tumour.

Figure 6 shows the simulation results for each of the four variables for the the homogeneous initial MM distribution at $t = 200$ time units. The tumour cell distribution shows a dead central region with

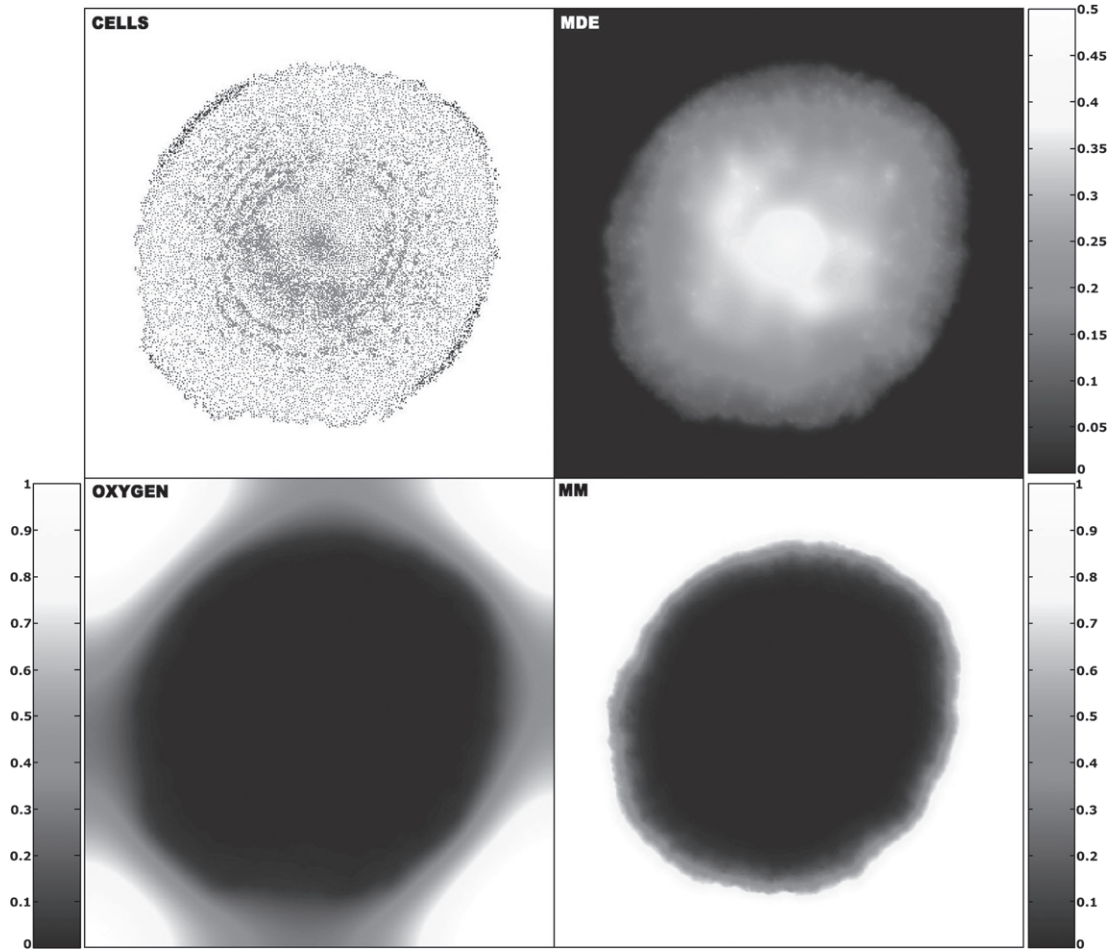


FIG. 6. Homogeneous tumour simulation results: spatial distribution of tumour cells, MDE, MM and oxygen (clockwise) at time $t = 200$ units (i.e. 200 generations, approximately 133 days). Colouration of the tumour shows the cell–cell adhesion value: dark grey ($A_i = 0$) and light grey represents dead cells. For the MDE, MM and oxygen concentration, the grey colour map is used, i.e. white = high concentration, black = low concentration and grey is in between. Note, a full colour version of this figure is available in the online publication.

a thin proliferating boundary. The dark coloured cells which have survived and continue to proliferate have the least adhesive phenotype, i.e. they have an adhesion value $A_i = 0$.

From Fig. 7 we can see the evolution of the tumour cell mutation population and note that there are approximately four phenotypes that dominate (mutation identification numbers [MID] being 25, 40, 55 and 88) the tumour population and survive most of the simulation. Of these phenotypes all have a zero cell adhesion value and two (MID 25, 88) have a short proliferation age (8.9 and 9.4 h, respectively) as well as high haptotaxis coefficients (3.9ρ and 2.4ρ , respectively). Interestingly, one of these phenotypes is the most dominant phenotype, always being expressed by the largest fraction of cells in the tumour population, and has the shortest proliferation age, highest haptotaxis coefficient, no cell–cell adhesion restrictions and, in contrast to the most aggressive type IV cells of the linear mutation model, one of

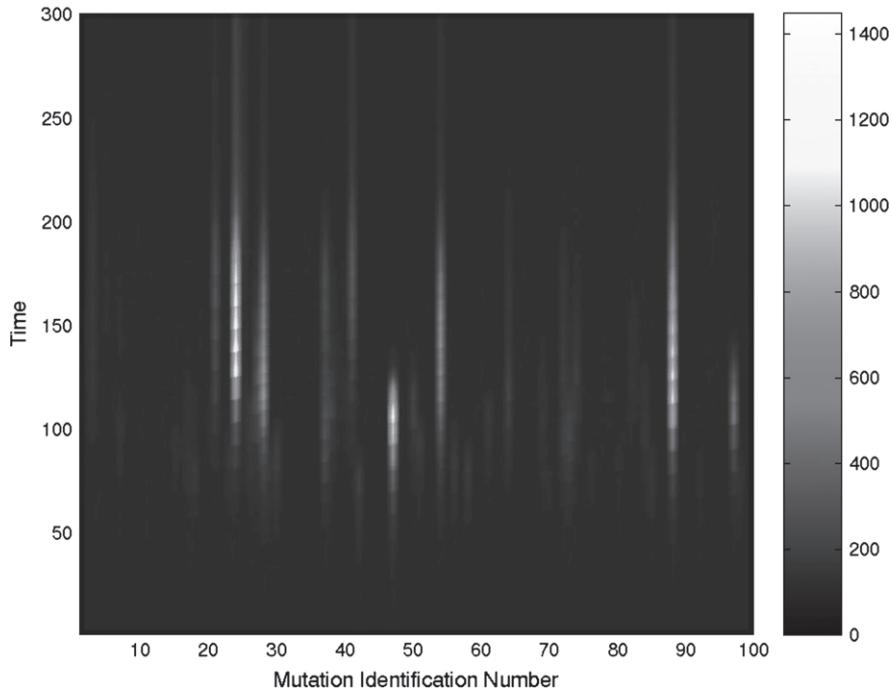


FIG. 7. Homogeneous tumour simulation results: evolution of mutation population. Colouration relates to cell numbers defined in the colour bar. Note, a full colour version of this figure is available in the online publication.

the smallest oxygen consumption rates. In some sense, through random mutation the most aggressive phenotype (in comparison with all 100 phenotypes) has been naturally selected.

Since the cells were invading through an initially homogeneous distribution of MM, we again see a more symmetric tumour (this symmetry is also seen in all three of the other variables). Comparing the tumour produced in Fig. 2 with the one in Fig. 6 it is clear that there is little difference geometrically between them. However, one has evolved from a linear mutation sequence of four phenotypes each progressively more aggressive and the other has evolved from a purely random sequence of 100 possible phenotypes. This implies that the geometry of the resulting tumour is governed more by cell–matrix interactions than cell–cell interactions as the common factor in these two simulations is the homogeneous matrix.

Figure 8 shows the simulation results for an initially random MM distribution. The tumour cell distribution is now radically different geometrically, showing a more fingered morphology, although it still consists of dead cells and a thin proliferating outer layer of cells. The same finger-like protrusions seen in Figs 3 and 4 for the linear mutations are again obtained for the random mutations. This certainly adds further weight to the hypothesis that tumour cell–matrix interactions are really what govern the evolving tumour geometry and as a result the actual MM distribution is an important factor in deciding how the tumour will grow.

The dark cells in Fig. 8 are mostly from one phenotype which has dominated the tumour population for the whole of the simulation. This is clearly seen from the evolution of the tumour cell population in Fig. 9. This phenotype (MID 15) has an adhesion value $A_i = 0$, a proliferation age of 8.2 h and a

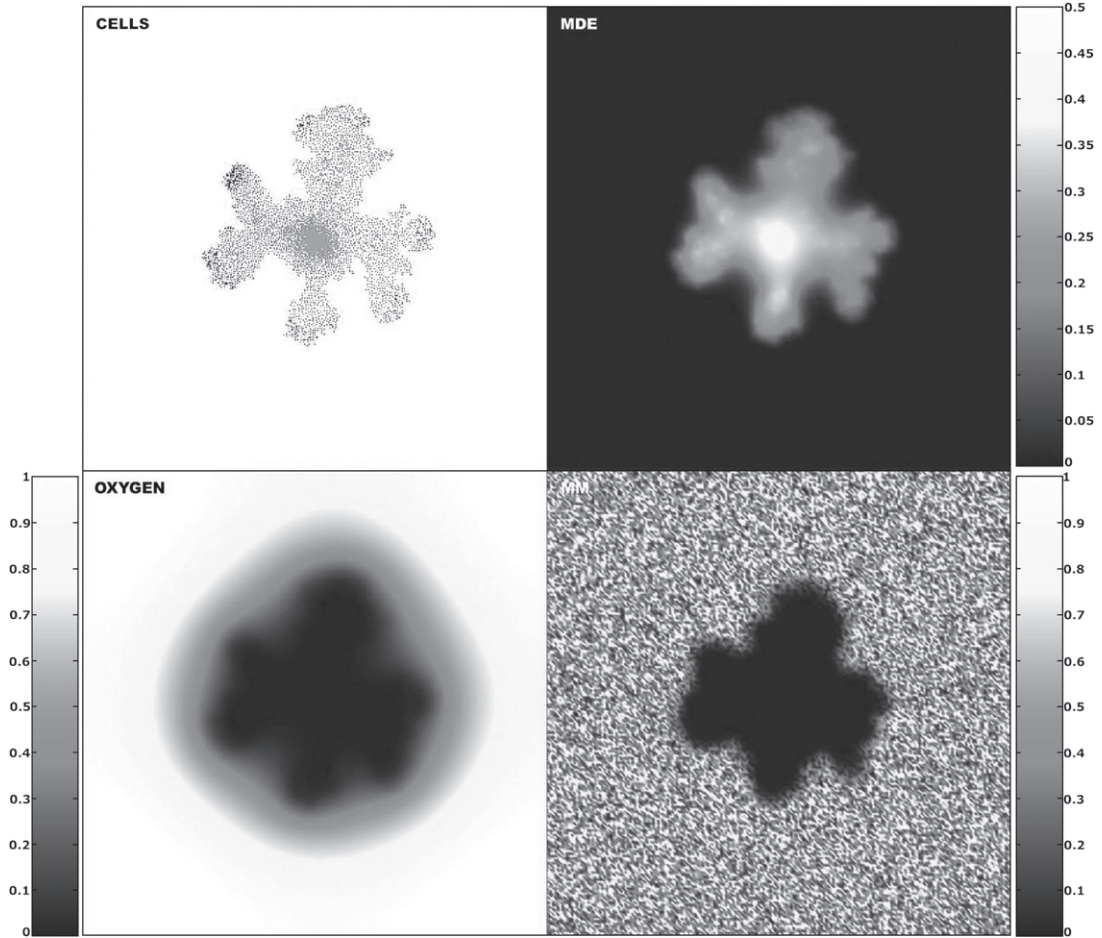


FIG. 8. Random tumour simulation results: spatial distribution of tumour cells, MDE, MM and oxygen (clockwise) at time $t = 200$ units (i.e. 200 generations, approximately 133 days). Colouration of tumour cells, MDE, MM and oxygen concentration is the same as in Fig. 5. Note, a full colour version of this figure is available in the online publication.

haptotaxis coefficient of 2.6ρ as well as a low oxygen consumption rate (approximately, 1.3ω). Again one of the most aggressive phenotypes has been naturally selected to lead the way for invasion at the boundary of the tumour. Since these cells have no cell–cell adhesion dependence, their migration is mainly driven by haptotaxis via the local MM gradients and it is these local gradients that ultimately define the tumour geometry.

The simulation that produced Fig. 8 and several other simulations (not shown), always resulted in only one or two main phenotypes completely dominating the tumour population. Whilst this result is only from a few runs, it would appear that tumours which evolved from the random MM distribution as opposed to the homogeneous MM distribution were more likely to have a single dominant phenotype. This might suggest that the MM heterogeneity somehow aids the more aggressive cells in dominating the tumour population, i.e. MM heterogeneity enhances natural selection.

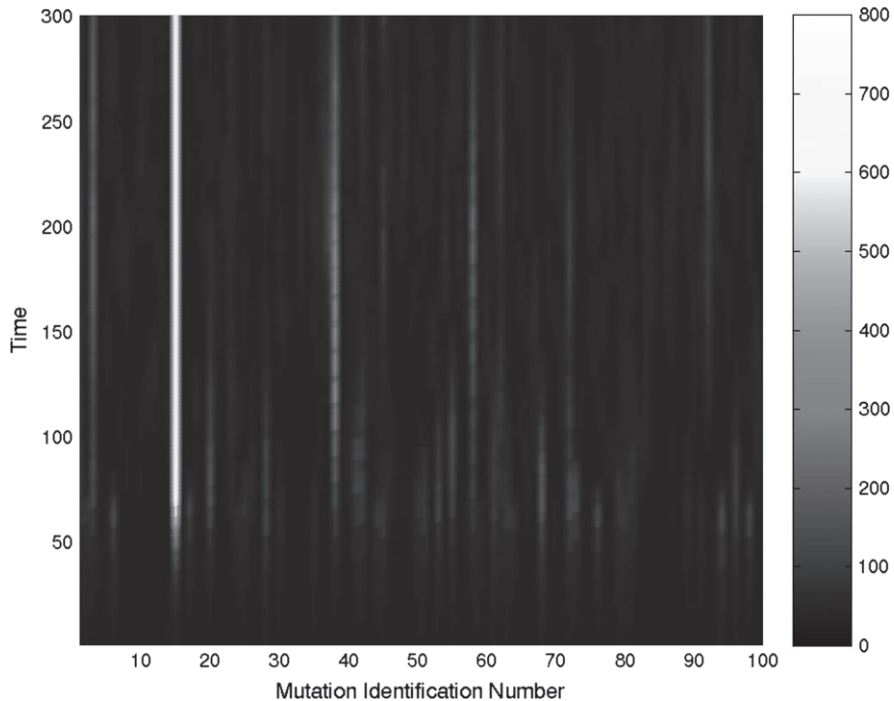


FIG. 9. Random tumour simulation results: evolution of mutation population. Colouration relates to cell numbers defined in the colour bar. Note, a full colour version of this figure is available in the online publication.

5. Discussion

In this paper we examined the effects of cell–cell and cell–matrix adhesion upon a growing invading tumour. In particular, we examined the effects of cell–matrix adhesion by considering three different initial matrix MM distributions, homogenous, heterogeneous and random. To examine the effects of cell–cell adhesion, we considered a heterogeneous tumour cell population that consisted of either four selected phenotypes each with different levels of cell–cell adhesion or 100 randomly selected phenotypes with random levels of adhesion. For the four selected phenotypes, we used a linear mutation sequence where all the cells are initially phenotype I (the least aggressive type with the highest cell–cell adhesion) and through mutation can become more aggressive via types II, III and IV (the most aggressive type with zero cell–cell adhesion). For the 100 phenotypes, we used a random mutation sequence where all the cells are initially assigned one of the 100 phenotypes randomly and through mutation another phenotype is selected randomly. Interestingly, whilst these two methods for considering tumour cell heterogeneity are very different they ultimately produced similar results.

The three simulations for the linear mutations (Figs 2–5) and the two simulations for the random mutations (Figs 6 and 8) use the same parameters, with the exception of the MM initial distributions and the way they consider mutation. These results illustrate the importance of tumour cell–matrix interactions in aiding or hindering the migration of individual cells that define the tumour geometry. This is dependent on the fact that the tumour cells must mutate to an aggressive phenotype in order to exploit the changes in local MM gradients. If the cell–cell adhesion parameters were to be fixed for all phenotypes (e.g. $A_i = 3$), then approximately the same small circular tumour would result for all MM

distributions. However, it is known that tumour cells lose the ability (via mutations) to recognise cell–cell adhesion molecules at an early stage in their development, e.g. E-cadherin is lost at an early stage of breast carcinogenesis and N-CAM loss in gliomas is associated with a high probability of metastasis (Takeichi, 1993).

Since the ECM is unlikely to contain a homogeneous distribution of MM, the homogeneous results (Figs 2 and 6) might be somewhat artificial. Similarly, the smooth heterogeneous MM (Fig. 3) is also somewhat unreal. Perhaps the most realistic MM would be the random distribution. Therefore, the results from the random tumour (Figs 4 and 8) represent the most realistic simulation, where the bias from the cell–matrix interactions is driven purely by local degradation of MM and subsequent creation of gradients which lead to directed migration of the tumour cells.

For the random mutation results, the fact that in most simulations the resulting tumour cell population consists of living cells with only one or two phenotypes might be surprising due to the random nature of the mutations. However, it seems logical to assume that it will be the most aggressive phenotypes that dominate the tumour population. Here aggressiveness would be defined as those phenotypes that have low proliferation age, zero cell–cell adhesion, a large haptotaxis coefficient and a low oxygen consumption rate. In comparison with the linear mutation results, we see little obvious difference in the resulting tumour cell distributions. Therefore, the assumption that the tumour cells always mutate to a more aggressive phenotype might not be so unrealistic. However, the definition of the aggressive phenotype (in the linear mutation model) includes higher oxygen consumption which is not seen in the random mutation results. This is logical, as phenotypes which live longer (due to consuming less oxygen) will be a part of the tumour population for a longer time. By linking certain phenotype properties, e.g. oxygen consumption with haptotaxis coefficient, then the lower oxygen consumption seen in the aggressive phenotypes of the random mutation model may not occur.

In conclusion, whilst cell–cell interactions are important at the early stages of a solid tumour's development, subsequent loss of cell–cell adhesion molecules (via mutation) results in tumour growth that is dominated by cell–matrix interactions. Therefore, these results predict that local tumour cell–matrix interactions are ultimately what control the overall geometry of the tumour and not the cell–cell interactions. In addition, cell–matrix interactions may also enhance natural selection, since the more random the MM distribution the more likely the most aggressive phenotype will be selected.

Much more work needs to be done in examining the range of behaviour that this model can display. In particular, the manner in which oxygen production is modelled needs to be refined perhaps by modelling more accurately the angiogenic network. There is certainly a need for a sensitivity analysis of the parameters, especially the mutation probabilities and the production/uptake parameters that are not known. The manner in which random mutation is modelled could be further refined so that a mutation resulted in only one aspect of the phenotype changing in a random manner, the daughter cells would then have some similarity with their parent. Nonetheless, the results presented above show the importance of considering both cell–cell and cell–matrix interactions in a model of tumour invasion and perhaps the strong dependence of the tumour geometry on local cell–matrix interactions points the way for future cancer research and treatment. In fact, recent research has focused on this very area; Hotary *et al.* (2003) have shown *in vitro* that the ECM can act like a cage constricting tumour growth, but once the tumour begins producing a specific MDE (MT1-MMP) it can escape the confines of the collagen fibres (that make up the ECM) by degrading them with the MDE.

Supplementary data

Figures 1 to 9 are available as colour images at imammb.oupjournals.org as supplementary data.

Acknowledgements

ARAA was supported by a Personal Research Fellowship from the Royal Society of Edinburgh and an equipment grant from the Royal Society of London. The author would also like to thank Prof. M. A. J. Chaplain for useful discussions and comments.

REFERENCES

- ANDERSON, A. R. A. (2003) A hybrid discrete-continuum technique for individual based migration models. *Polymer and Cell Dynamics* (W. Alt, M. Chaplain, M. Griebel & J. Lenz eds). Basel, Switzerland: Birkhauser.
- ANDERSON, A. R. A. & CHAPLAIN, M. A. J. (1998) Continuous and discrete mathematical models of tumour-induced angiogenesis. *Bull. Math. Biol.*, **60**, 857–899.
- ANDERSON, A. R. A., CHAPLAIN, M. A. J., NEWMAN, E. L., STEELE, R. J. C. & THOMPSON, A. M. (2000) Mathematical modelling of tumour invasion and metastasis. *J. Theor. Med.*, **2**, 129–154.
- ANDERSON, A. R. A. & PITCAIRN, A. (2003) Application of the hybrid discrete-continuum technique. *Polymer and Cell Dynamics* (W. Alt, M. Chaplain, M. Griebel & J. Lenz eds). Basel, Switzerland: Birkhauser.
- ANDERSON, A. R. A., SLEEMAN, B. D., YOUNG, I. M. & GRIFFITHS, B. S. (1997) Nematode movement along a chemical gradient in a structurally heterogeneous environment: II. Theory. *Fundam. Appl. Nematol.*, **20**, 165–172.
- BARNES, D. E., LINDAHL, T. & SEDGWICK, B. (1993) DNA repair. *Curr. Opin. Cell Biol.*, **5**, 424–433.
- BOYLE, J. O., HAKIM, J. & KOCH, W. (1993) The incidence of p53 mutations increases with progression of head and neck cancer. *Cancer Res.*, **53**, 4477–4480.
- BRAY, D. (1992) *Cell Movements*. New York: Garland Publishing.
- BURRIDGE, K. & CHRZANOWSKA-WODNICKA, M. (1996) Focal adhesions, contractability, and signalling. *Annu. Rev. Cell Dev. Biol.*, **12**, 463–518.
- BYRNE, H. M., CHAPLAIN, M. A. J., PETTET, G. J. & MCELWAIN, D. L. S. (1999) A mathematical model of trophoblast invasion. *J. Theor. Med.*, **1**, 275–286.
- CALABRESI, P. & SCHEIN, P. S. (eds) (1993) *Medical Oncology*, 2nd edn. New York: McGraw-Hill.
- CARTER, S. B. (1965) Principles of cell motility: the direction of cell movement and cancer invasion. *Nature*, **208**, 1183–1187.
- CHAMBERS, A. F. & MATRISIAN, L. M. (1997) Changing views of the role of matrix metalloproteinases in metastasis. *J. Natl. Cancer Inst.*, **89**, 1260–1270.
- CLARK, E. A. & BRUGGE, J. S. (1995) Integrins and signal transduction pathways: the road taken. *Science*, **268**, 233–239.
- CASCIARI, J. J., SOTIRCHOS, S. V. & SUTHERLAND, R. M. (1992) Variation in tumour cell growth rates and metabolism with oxygen-concentration, glucose-concentration and extracellular pH. *J. Cell. Physiol.*, **151**, 386–394.
- CHAPLAIN, M. A. J. (1996) Avascular growth, angiogenesis and vascular growth in solid tumours: the mathematical modelling of the stages of tumour development. *Math. Comput. Model.*, **23**, 47–87.
- CHAPLAIN, M. A. J. & SLEEMAN, B. D. (1993) Modelling the growth of solid tumours and incorporating a method for their classification using nonlinear elasticity theory. *J. Math. Biol.*, **31**, 431–479.
- DEBRUYNE, P. R., BRUYNEEL, E. A. & KARAGUNI, I.-M. *et al.* (2002) Bile acids stimulate invasion and haptotaxis in human colorectal cancer cells through activation of multiple oncogenic signalling pathways. *Oncogene*, **21**, 6740–6750.
- DORMANN, S. & DEUTSCH, A. (2002) Modeling of self-organized avascular tumor growth with a hybrid cellular automaton. *In Silico Biol.*, **2**, 0035.
- DÜCHTING, W. (1990) Tumor growth simulation. *Comput. Graph.*, **14**, 505–508.
- DÜCHTING, W., ULMER, W. & GINSBERG, T. (1996) Cancer: a challenge for control theory and computer modelling. *Eur. J. Cancer*, **32A**, 1283–1292.

- FREYER, J. P., TUSTANOFF, E., FRANKO, A. J. & SUTHERLAND, R. M. (1984) In situ consumption rates of cells in v-79 multicellular spheroids during growth. *J. Cell. Physiol.*, **118**, 53–61.
- FOLKMAN, J. & HOCHBERG, M. (1973) Self-regulation of growth in three dimensions. *J. Exp. Med.*, **138**, 745–753.
- GATENBY, R. A. & GAWLINSKI, E. T. (1996) A reaction–diffusion model of cancer invasion. *Cancer Res.*, **56**, 5745–5753.
- HOTARY, K., ALLEN, E. D., BROOKS, P. C., DATTA, N. S., LONG, M. W. & WEISS, S. J. (2003) Membrane type 1 matrix metalloproteinase usurps tumour growth control imposed by the three-dimensional extracellular matrix. *Cell*, **114**, 33–45.
- HOTARY, K., ALLEN, E. D., PUNTURIERI, A., YANA, I. & WEISS, S. J. (2000) Regulation of cell invasion and morphogenesis in a 3-dimensional type I collagen matrix by membrane-type metalloproteinases 1, 2 and 3. *J. Cell Biol.*, **149**, 1309–1323.
- HYNES, R. O. (1992) Integrins: versatility, modulation, and signalling in cell adhesion. *Cell*, **69**, 11–25.
- JOHANSSON, N., AHONEN, M. & KAHARI, V.-M. (2000) Matrix metalloproteinases in tumour invasion. *Cell. Mol. Life Sci.*, **57**, 5–15.
- KANSAL, A. R., TORQUATO, S., HARSH, G. R., CHIOCCA, E. A. & DEISBOECK, T. S. (2000) Simulated brain tumor growth using a three-dimensional cellular automaton. *J. Theor. Biol.*, **203**, 367–382.
- KIMMEL, M. & AXELROD, D. E. (1991) Unequal cell division, growth regulation and colony size of mammalian cells: a mathematical model and analysis of experimental data. *J. Theor. Biol.*, **153**, 157–180.
- KLOMINEK, J., ROBERT, K. H. & SUNDQVIST, K.-G. (1993) Chemotaxis and haptotaxis of human malignant mesothelioma cells: effects of fibronectin, laminin, type IV collagen, and an autocrine motility factor-like substance. *Cancer Res.*, **53**, 4376–4382.
- KOOCHEKPOUR, S., PILKINGTON, G. J. & MERZAK, A. (1995) Hyaluronic acid/CD44H interaction induces cell detachment and stimulates migration and invasion of human glioma cells in vitro. *Int. J. Cancer*, **63**, 450–454.
- LACOVARA, J., CRAMER, E. B. & QUIGLEY, J. P. (1984) Fibronectin enhancement of directed migration of B16 melanoma cells. *Cancer Res.*, **44**, 1657–1663.
- LANE, D. P. (1994) The regulation of p53 function. Steiner Award Lecture. *Int. J. Cancer*, **57**, 623–627.
- LAWRENCE, J. A. & STEEG, P. S. (1996) Mechanisms of tumour invasion and metastasis. *World J. Urol.*, **14**, 124–130.
- LIOTTA, L. A., RAO, C. N. & BARSKY, S. H. (1983) Tumour invasion and the extracellular matrix. *Lab. Invest.*, **49**, 636–649.
- MARUSIC, M., BAJZER, Z., FREYER, J. P. & VUK-PAVLOVIC, S. (1994) Analysis of growth of multicellular tumour spheroids by mathematical models. *Cell Prolif.*, **27**, 73–94.
- MATRISIAN, L. M. (1992) The matrix-degrading metalloproteinases. *Bioessays*, **14**, 455–463.
- MCCARTHY, J. B. & FURCHT, L. T. (1984) Laminin and fibronectin promote the directed migration of B16 melanoma cells in vitro. *J. Cell Biol.*, **98**, 1474–1480.
- MELICOW, M. M. (1982) The three-steps to cancer: a new concept of carcinogenesis. *J. Theor. Biol.*, **94**, 471–511.
- MIGNATTI, P. & RIFKIN, D. B. (1993) Biology and biochemistry of proteinases in tumor invasion. *Physiol. Rev.*, **73**, 161–195.
- ORME, M. E. & CHAPLAIN, M. A. J. (1996) A mathematical model of vascular tumour growth and invasion. *Math. Comput. Model.*, **23**, 43–60.
- OTHMER, H. & STEVENS, A. (1997) Aggregation, blowup and collapse: the ABCs of taxis and reinforced random walks. *SIAM J. Appl. Math.*, **57**, 1044–1081.
- PERUMPANANI, A. J., SHERRATT, J. A., NORBURY, J. & BYRNE, H. M. (1996) Biological inferences from a mathematical model of malignant invasion. *Invasion Metastasis*, **16**, 209–221.
- QI, A., ZHENG, X., DU, C. & AN, B. (1993) A cellular automaton model of cancerous growth. *J. Theor. Biol.*, **161**, 1–12.
- QUIGLEY, J. P., LACOVARA, J. & CRAMER, E. B. (1983) The directed migration of B-16 melanoma-cells in response to a haptotactic chemotactic gradient of fibronectin. *J. Cell Biol.*, **97**, A450–A451.

- RADOTRA, B., MCCORMICK, D. & COCKARD, A. (1994) CD44 plays a role in adhesive interactions between glioma cells and extracellular matrix components. *Neuropathol. Appl. Neurobiol.*, **20**, 399–405.
- RETSKY, M. W., SWARTZENDRUBER, D. E., WARDWELL, R. H. & BAME, P. D. (1990) Is gompertzian or exponential kinetics a valid description of individual human cancer growth? *Med. Hypotheses*, **33**, 95–106.
- SHERRATT, J. A. & NOWAK, M. A. (1992) Oncogenes, anti-oncogenes and the immune response to cancer: a mathematical model. *Proc. R. Soc. Lond. B*, **248**, 261–271.
- SHERWOOD, L. (2001) *Human Physiology: From Cells to Systems*, 4th edn. Pacific Grove, California: Brooks/Cole.
- SLEE, E. A., O'CONNOR, D. J. & LU, X. (2004) To die or not to die: how does p53 decide? *Oncogene*, **23**, 2809–2818.
- SMOLLE, J. & STETTNER, H. (1993) Computer simulation of tumour cell invasion by a stochastic growth model. *J. Theor. Biol.*, **160**, 63–72.
- STETLER-STEVENSON, W. G., AZNAVOORIAN, S. & LIOTTA, L. A. (1993) Tumor cell interactions with the extracellular matrix during invasion and metastasis. *Annu. Rev. Cell Biol.*, **9**, 541–573.
- STETLER-STEVENSON, W. G., HEWITT, R. & CORCORAN, M. (1996) Matrix metallo-proteinases and tumour invasion: from correlation to causality to the clinic. *Cancer Biol.*, **7**, 147–154.
- TAKEICHI, M. (1993) Cadherins in cancer: implications for invasion and metastasis. *Curr. Opin. Cell Biol.*, **5**, 806–811.
- TERRANOVA, V. P., DIFLORIO, R., LYALL, R. M., HIC, S., FRIESEL, R. & MACIAG, T. (1985) Human endothelial cells are chemotactic to endothelial cell growth factor and heparin. *J. Cell Biol.*, **101**, 2330–2334.
- THORGEIRSSON, U. P., LINDSAY, C. K., COTTAM, D. W. & GOMEZ, D. E. (1994) Tumor invasion, proteolysis, and angiogenesis. *J. Neurooncol.*, **18**, 89–103.
- TRACQUI, P. (1995) From passive diffusion to active cellular migration in mathematical models of tumour invasion. *Acta Biotheor.*, **43**, 443–464.
- WARD, J. P. & KING, J. R. (1999) Mathematical modelling of avascular-tumour growth II: modelling growth saturation. *IMA J. Math. Appl. Med. Biol.*, **16**, 171–211.
- WHELDON, T. E. (1986) Mathematical models in experimental and clinical oncology. *Mathematical Methods in Medicine* (D. Ingram & R. F. Bloch eds). London: J. Wiley & Sons, pp. 1–32.
- ZERVOUDAKI, A., ECONOMOU, E., PITSAVOS, C., VASILIADOU, K. *et al.* (2004) The effect of Ca²⁺ channel antagonists on plasma concentrations of matrix metalloproteinase-2 and -9 in essential hypertension. *Am. J. Hypertens.*, **17**, 273–276.